J. Fluid Mech. (1991), *vol.* 228, *pp.* 607–628
Printed in Great Britain

Vacillatory convection in a rotating spherical fluid shell at infinite Prandtl number

By KEKE ZHANG
Department of Earth Sciences, University of Leeds, Leeds, LS2 9JT, UK

(Received 7 March 1990 and in revised form 17 December 1990)

The temporal and spatial behaviour of three-dimensional convection at infinite Prandtl number, in a rotating spherical fluid shell of radius ratio $\eta = r_i/r_o = 0.4$, has been investigated numerically for a range of Taylor number for which $m_c = 2$, 3 and 4 are the critical values of azimuthal wavenumber at the onset of convection. When the Rayleigh number, R, exceeds a critical value, R_{1c}, primary nonlinear solutions with the predominant wavenumber $m_0 = 4$ in the form of azimuthally travelling waves give way to secondary solutions in the form of steadily drifting mixed-mode convection with two predominant wavenumbers, $m_0 = 2$ and 4. The secondary bifurcation solution becomes unstable at another critical value, R_{2c}, that leads to the tertiary solution in which the dominant wavelength of convection vacillates periodically between the two competing scales characterized by the azimuthal wavenumbers $m_0 = 2$ and 4. Instabilities and bifurcations associated with the evolution from a static state to wavenumber vacillation are discussed for a representative Taylor number of $T = 10^4$. It is also shown that the interaction between the two spatially resonant wavenumbers $m = 2$ and 4 is much stronger than the interaction between the non-resonant wavenumbers $m = 3$ and 4 even though $R_c(m = 3)$ is much closer to $R_c(m = 4)$ than $R_c(m = 2)$. For the convection of the dominant wavenumber $m_0 = 2$, the analysis is focused on the range of Taylor number $T > T_4$, where T_4 is the Taylor number at which the critical wavenumber m_c changes from 2 to 4 at the onset of convection. The $m_0 = 2$ steadily drifting nonlinear solutions, which are unstable at small amplitudes owing to the Eckhaus-type instability, gain their stability at large amplitudes at R_{1c} through nonlinear effects, and lose their stability at a higher Rayleigh number, R_{2c}, to the amplitude-vacillating instability which leads to a periodic change in the amplitude of convection with little fluctuation in the pattern of flow.

1. Introduction

Buoyancy-driven convection in rotating spherical systems is associated with many basic geophysical and astrophysical processes in planetary fluid cores as well as in the atmospheres of the major planets. The understanding of convection in a rotating spherical shell is an essential step towards a full nonlinear theory of planetary dynamos (Zhang, Busse & Hircshing 1989). In fact, a nonlinear magnetohydrodynamic dynamo solution can be treated as a new bifurcation branch in connection with a nonlinear convection solution. Such bifurcation analysis has been successfully used to obtain the full nonlinear dynamo solutions in a rotating spherical fluid shell (Zhang & Busse 1988, 1989, 1990). Interest in convection in the limit of infinite Prandtl number is particularly motivated by the compositional convection

in the Earth's core which is likely to drive the geodynamo (Braginsky 1963; Gubbins 1977; Loper 1978). Furthermore, the limit of infinite Prandtl number forms the mathematically simplest and yet physically well-posed convection problem for rotating spherical systems. The interpretation of heat flux as the flux of light constituents, as well as the other motivations of studying the problem, has been particularly discussed in the previous work by Zhang & Busse (1990).

Apart from its many geophysical and astrophysical applications, rotating spherical convection is of interest in fluid dynamics in general. Understanding of convection in a fluid layer heated from below has been fundamental in improving our understanding of complicated behaviour in fluid dynamic systems. We refer to Busse (1978) for a general discussion. Although a plane fluid layer provides a simple fluid dynamic system, the evolution of the pattern cannot be theoretically investigated readily because a continuous band of infinite modes in the neighbourhood of the critical mode may be excited. In contrast, a rotating spherical fluid system has the advantage over a plane fluid layer in having the discrete integer wavenumbers arising from the spherical geometry and a small number of the excitable azimuthal wavenumbers in the neighbourhood of the critical mode arising from the influence of rotation. In addition, the time dependence of spherical convection in the form of azimuthally travelling waves appears at the onset of convection. However, the problem of convection in a rotating system with spherical geometry is very complicated. As a result of the coupling of spherical harmonics by the Coriolis force and the phase shift of convection rolls caused by spherical geometry, linear solutions in the form of either

$$u \sim F(s)\,G(z)\,\exp\,(\mathrm{i}\omega t + \mathrm{i}m\phi),$$

or

$$u \sim F(r)\,G(\theta)\,\exp\,(\mathrm{i}\omega t + \mathrm{i}m\phi),$$

corresponding to spherical cylindrical and polar coordinates respectively, are, in general, not permitted (Zhang 1991). The appropriate normal-form equations for a rotating spherical system are not feasible, and even linear analysis inevitably requires a numerical treatment. Furthermore, the linear solutions obtained from numerical analysis are complex, and cannot be approximately represented by a small number of modes. It is for this reason that the analytical approach widely adopted for the similar problems of other simple geometries such as a plane layer appears difficult to apply to the problem treated in this paper. This paper presents the first attempt at determining the convective transitions from the first instability to spatially and temporally more complex convection flows in a rotating system with spherical geometry.

Nonlinear convection in rotating spherical geometries has demonstrated complex temporal and spatial structures in direct numerical simulations for the solar convection zone at high Rayleigh numbers (Gilman 1977; Hart, Glatzmaier & Toomre 1986) and experimental investigations in the laboratory (Carrigan & Busse 1983; Chamberlain & Carrigan 1986), and in the space shuttle Challenger (Hart *et al.* 1986). Much of the behaviour is connected with the combined effects of spherical geometry and rotation, and is not currently understood. We have chosen the numerical bifurcation approach to tackle this nonlinear spherical convection problem with the aim of comprehending the basic instabilities and bifurcations which lead to the intricate behaviour of rotating spherical convection. The domain of parameters of the problem is restricted to one where convergent solutions can be obtained. Although the Taylor numbers considered are not sufficiently high for a realistic geophysical situation, which is not accessible because of our numerical approach and

the limitations of computer power, the primary effects of rotation on the convection are sufficiently large to illuminate the most important interaction imposed by the constraint of rotation and the nonlinearity of convection.

Our discussions will be mainly concentrated on the second and third instabilities and the associated nonlinear bifurcation solutions at two representative Taylor numbers, $T = 1.2 \times 10^3$ and 10^4, though the whole range of Taylor numbers $0 < T < 10^5$ has been investigated. The critical azimuthal wavenumbers for the onset of convection are $m_c = 2$ and 4 for $T = 1.2 \times 10^3$ and 10^4 respectively. The main features of the relationship of instabilities as well as their boundaries versus Rayleigh number R in their initial bifurcations are determined at these two Taylor numbers. We shall explore the transition from a relatively simple three-dimensional pattern with steadily drifting convective cells to a more complicated spatial pattern of mixed-mode drifting convection. We shall also examine the stability of steadily drifting mixed-mode convection, and investigate the transition from the drifting mixed-mode convection to wavenumber-vacillating convection. (The term *vacillation* was used by Hide (1958) to describe a steady repeating fluctuation of the drifting flow observed experimentally in a rotating cylindrical fluid system.) In particular, we will focus on how changes in the spatial structure of convection cells lead to a variation in temporal behaviour of the convection. Of particular interest is the stability behaviour of $m_0 = 2$ solutions, manifested in the competitive influences on the system of rotation and nonlinearity, where m_0 denotes the azimuthal wavenumber of predominant modes for a nonlinear solution. It will be shown that it is possible for the system at finite amplitudes to select the small wavenumber even when the large wavenumber is much more preferred on the basis of the linear stability analysis for the onset of convection. It is also shown that the interaction between the two spatially resonant wavenumbers $m = 2$ and 4 is dominant over the interaction between the non-resonant wavenumbers $m = 3$ and 4 even though the critical Rayleigh number $R_c(m = 3)$ is much closer to $R_c(m = 4)$ than $R_c(m = 2)$.

The remainder of the paper is laid out as follows. After presenting the mathematical formulation of the problem in §2, the onset of the first instability and the corresponding bifurcation solutions of nonlinear convection are briefly discussed in §3. The results of linear stability analysis for nonlinear steadily drifting solutions will be presented in §4. Stationary bifurcation solutions for mixed-mode convection as well as its stability properties will be shown in §5. In §6, vacillating tertiary solutions of nonlinear convection are described. The paper closes in §7 with the summary and discussion of the main features of our analysis.

2. Mathematical formulation and method

We consider nonlinear convection in a fluid spherical shell of constant thermal diffusivity, κ, constant coefficient of thermal expansion, α, and constant viscosity, ν. The whole system is rotating with a constant angular velocity $\boldsymbol{\Omega}$ in the presence of its own gravitational field. The simplest heating model (Chandrasekhar 1961; Roberts 1968) in which the purely conductive state

$$\nabla T_s = -\beta r,$$

where β is a constant, is produced by a uniform distribution of heat sources, is adopted. The fluid is assumed to be Boussinesq, consequently the velocity field can be written as a sum of poloidal and toroidal vectors

$$\boldsymbol{u} = \nabla \times \nabla \times \boldsymbol{r}v + \nabla \times \boldsymbol{r}w.$$

By adopting $d = r_o - r_i$, d^2/κ, and βd^2 as scales of length, time, and temperature of the system respectively, it follows that the governing non-dimensional scalar equations are

$$\left[\left(\nabla^2 - \frac{1}{Pr}\frac{\partial}{\partial t}\right)\mathrm{L}_2 + \tau\frac{\partial}{\partial\phi}\right]\nabla^2 v + \tau\mathrm{Q}w - R\mathrm{L}_2\Theta = -\frac{\boldsymbol{r}}{Pr}\cdot\nabla\times\nabla\times(\boldsymbol{u}\cdot\nabla\boldsymbol{u}), \tag{1}$$

$$\left[\left(\nabla^2 - \frac{1}{Pr}\frac{\partial}{\partial t}\right)\mathrm{L}_2 + \tau\frac{\partial}{\partial\phi}\right]w - \tau\mathrm{Q}v = \frac{\boldsymbol{r}}{Pr}\cdot\nabla\times(\boldsymbol{u}\cdot\nabla\boldsymbol{u}), \tag{2}$$

$$\left(\nabla^2 - \frac{\partial}{\partial t}\right)\Theta + \mathrm{L}_2 v = \boldsymbol{u}\cdot\nabla\Theta, \tag{3}$$

where the temperature deviation from T_s is denoted by Θ. In spherical polar coordinates (r, θ, ϕ) with the polar axis in the direction of rotation, the operator L_2, the negative Laplacian on the unit sphere, is defined as

$$\mathrm{L}_2 = -r^2\nabla^2 + \frac{\partial}{\partial r}r^2\frac{\partial}{\partial r}.$$

The differential operator Q introduced by Roberts (1968) is

$$\mathrm{Q} = \boldsymbol{k}\cdot\nabla - \tfrac{1}{2}(\mathrm{L}_2\boldsymbol{k}\cdot\nabla + \boldsymbol{k}\cdot\nabla\mathrm{L}_2),$$

where $\boldsymbol{k}$ is an unit vector parallel to the axis of rotation. The system (1)–(3) is characterized by three dimensionless parameters, the Rayleigh number R, the Prandtl number Pr and the Taylor number T, defined as

$$R = \frac{\alpha\beta\gamma d^6}{\nu\kappa}, \quad Pr = \frac{\nu}{\kappa}, \quad T = \tau^2 = \left(\frac{2\Omega d^2}{\nu}\right)^2.$$

Henceforth, all variables will be presented in dimensionless form. In the limit of infinite Prandtl number Pr, the only nonlinearity of the problem is produced by the advection term in (3). The assumptions of impenetrable, perfectly thermal conducting, and stress-free boundaries impose the following conditions at the inner and outer bounding spherical surfaces:

$$v = \Theta = \frac{\partial^2 v}{\partial r^2} = \frac{\partial}{\partial r}\left(\frac{w}{r}\right) = 0$$

at $r_i = \eta/(1-\eta)$ and $r_o = 1/(1-\eta)$, where η is chosen equal to 0.4 throughout, which is appropriate for the Earth's core. The boundary condition $\partial\Theta/\partial r = 0$ at $r = r_o$ (which is more appropriate for modelling convection driven by chemical buoyancy) was not chosen so that a comparison with earlier studies of the same model with moderate Prandtl numbers can be readily made.

The Galerkin spectral method is employed in our numerical analysis. The three dependent variables are represented in terms of complete systems of functions with the radial functions satisfying the boundary conditions,

$$\Theta = \sum_{l,m,n} \Theta_{lmn} \sin n\pi(r - r_i)\, Y_l^m(\theta, \phi - ct) + \text{c.c.},$$

$$v = \sum_{l,m,n} v_{lmn} \sin n\pi(r - r_i)\, Y_l^m(\theta, \phi - ct) + \text{c.c.},$$

$$w = \sum_{l,m,n} w_{lmn}\, r \cos n\pi(r - r_i)\, Y_l^m(\theta, \phi - ct) + \text{c.c.},$$

where c is the drift rate of a solution. The coefficients Θ_{lmn}, v_{lmn} and w_{lmn} are complex and time independent for steadily drifting solutions, but they are function of the time

t in the case of vacillating convection. The c.c. denote complex conjugate, which should be included in the expansions for nonlinear solutions and excluded for linear calculations such as linear stability analysis. For obtaining an approximate numerical solution, we have introduced the triangular truncation scheme in which all coefficients with indices satisfying

$$l-jm_0+2n+2j > 2N_t+3$$

are neglected, where $m = jm_0$, and m_0 is usually related to the dominant azimuthal wavenumber of a nonlinear solution. Most of the calculations reported in this paper use the truncation parameter $N_t = 4$ which is sufficient at least for accuracies of order 5% for the parameter range treated. The results were verified by increasing the spatial resolution of the solutions as we will discuss in the text.

The analysis is conducted in four stages. First, the convective instability in terms of the critical parameters R_c, T, m_c is analysed. The linear results can serve as an important guide for choosing parameters, such as the predominant wavenumber, in the computation of primary nonlinear solutions. In the second stage, the primary solutions describing steadily azimuthally drifting rolls of convection are calculated with a Newton–Raphson iteration scheme. For the third stage, stability of the primary solutions is investigated by superimposing infinitesimal three-dimensional general perturbations such as

$$\tilde{\Theta} = \sum_{l,m,n} \tilde{\Theta}_{lmn} \sin n\pi(r-r_i)\, Y_l^m(\theta, \phi - ct) \exp(\mathrm{i}M\phi + \sigma t),$$

onto the steadily drifting solution, where $\exp(\mathrm{i}M\phi)$ is the Floquet factor, and the parameter M is an integer which varies between 0 and $m_0 - 1$. Similar expansions are assumed for the velocity fields v and w. The disturbances are truncated at the same level as for the corresponding nonlinear solution. By neglecting self-interactions of the perturbations, and subtracting the equations for the steadily drifting solution, the perturbed system is described by the following linear homogeneous equations:

$$\left[\nabla^2 \mathrm{L}_2 + \tau \frac{\partial}{\partial \phi}\right] \nabla^2 \tilde{v} + \tau \mathrm{Q} \tilde{w} - R \mathrm{L}_2 \tilde{\Theta} = 0, \tag{4}$$

$$\left[\nabla^2 \mathrm{L}_2 + \tau \frac{\partial}{\partial \phi}\right] \tilde{w} - \tau \mathrm{Q} \tilde{v} = 0, \tag{5}$$

$$(\nabla^2 - \sigma + \mathrm{i}c)\tilde{\Theta} + \mathrm{L}_2 \tilde{v} = \boldsymbol{u} \cdot \nabla \tilde{\Theta} + \tilde{\boldsymbol{u}} \cdot \nabla \Theta. \tag{6}$$

These equations form an eigenvalue problem with eigenvalue $\sigma = \sigma_r + \mathrm{i}\sigma_i$. The largest real part of σ represents either the growth or decay rate of the disturbance, that is, stability of the nonlinear convection flow. The imaginary part of the eigenvalue usually suggests either a steady or an oscillatory bifurcation of the new solution. If the imaginary part of σ is zero, the new branch of nonlinear convection corresponding to the instability may be obtained by the same procedure as in stage two. Otherwise, vacillating convection solutions are found by time-integration of (1)–(3) with the implicit Crank–Nicolson scheme.

3. Onset of convection and primary nonlinear solutions

Owing to the rotational constraint, the critical Rayleigh number R_c and critical wavenumber m_c required for convective instabilities increase with the asymptotic law (Roberts 1968; Busse 1970)

$$R_c = O(T^{\frac{2}{3}}), \quad m_c = O(T^{\frac{1}{6}})$$

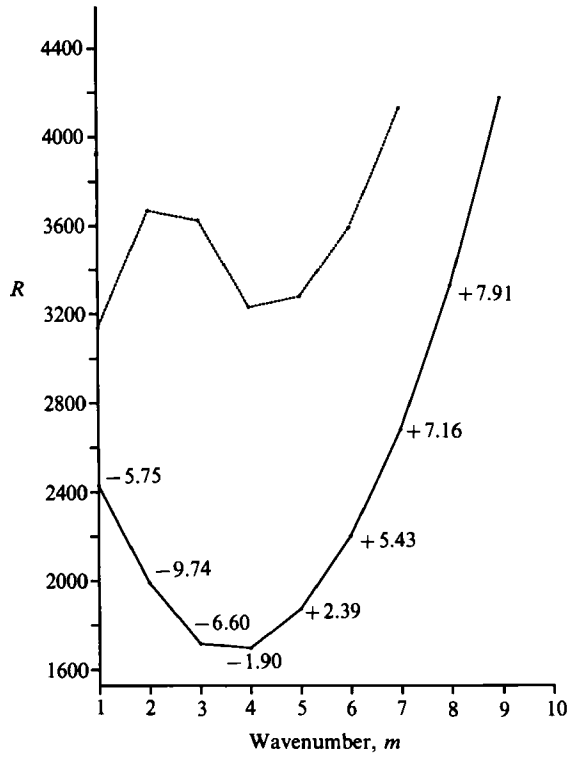

FIGURE 1. Instability curves at $T = 10^4$ are shown for both the equatorially symmetric (solid line) and antisymmetric (dotted line) modes. The numbers indicate the oscillation frequencies at the onset of convection for the corresponding wavenumber.

at large Taylor number. At a particular Taylor number, the preferred scale of motion described by an azimuthal wavenumber provides a sufficient pressure gradient to balance the Coriolis force with minimum dissipation. The instability curves in the range of azimuthal wavenumbers m from 1 to 9 with respect to both the equatorially symmetric mode

$$(u_r, u_\theta, u_\phi)(r, \theta, \phi) = (u_r, -u_\theta, u_\phi)(r, \pi-\theta, \phi),$$

and the equatorially antisymmetric mode

$$(u_r, u_\theta, u_\phi)(r, \theta, \phi) = (-u_r, u_\theta, -u_\phi)(r, \pi-\theta, \phi),$$

are illustrated in figure 1 for $T = 10^4$. It is clear that the wavenumber $m = 4$ is at the minimum of the marginal stability curve,

$$R_c(m = 2) > R_c(m = 5) > R_c(m = 3) > R_c(m = 4).$$

It is of interest to note that owing to the combined effects of spherical boundaries and rotation, the form of convective instability is a travelling wave propagating in the azimuthal direction that is determined by the value of Taylor number, T, and the azimuthal wavenumber (Gilman 1975). In contrast to the non-rotating convection, an important feature of the finite-amplitude solution is a steady drift of the whole pattern relative to the rotating frame. Primary bifurcation solutions can, however, be made steady if we transform from the rotating frame to a reference frame moving with the drifting rate of convection, c. This form of motion will be referred to as steadily drifting convection.

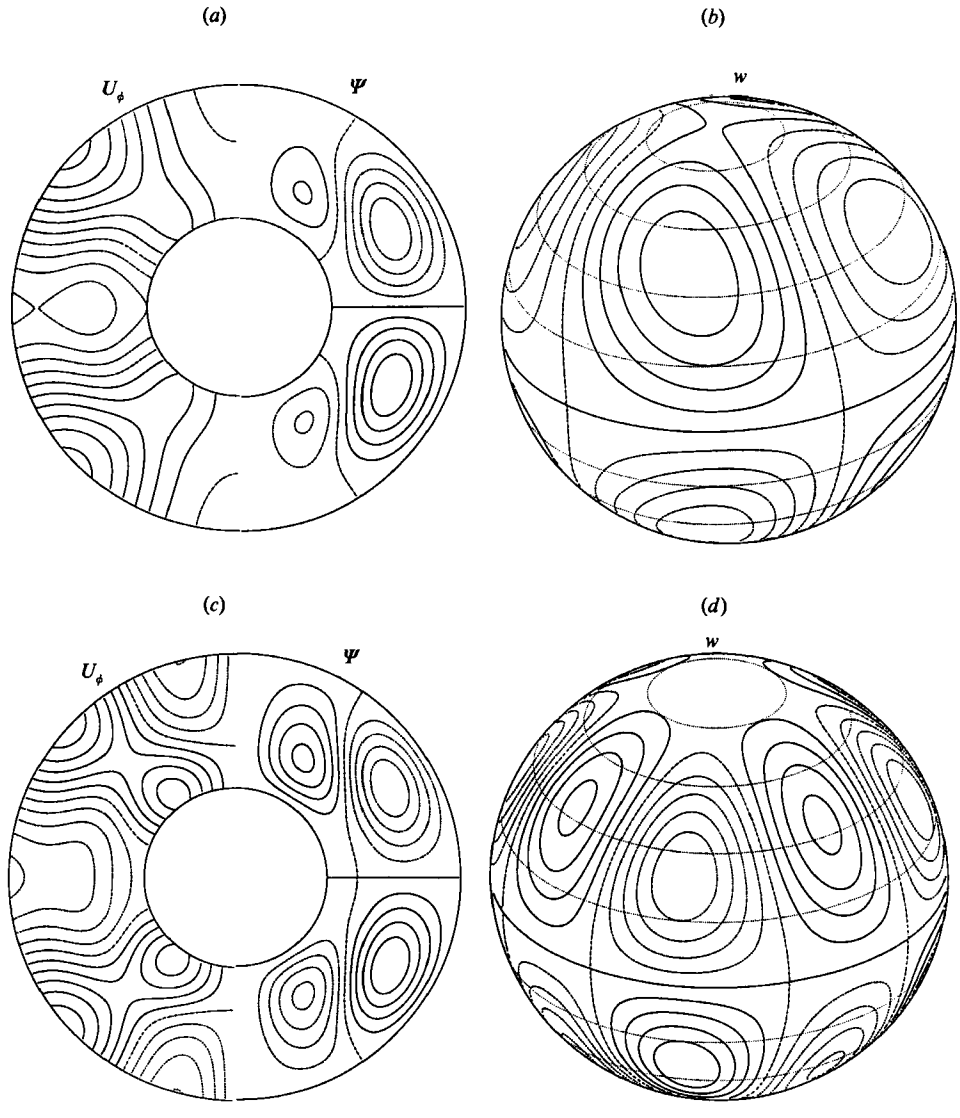

FIGURE 2. (*a*) Meridional circulation (on the right-hand side), and contours of the differential rotation (on the left-hand side) in a meridional cross-section, and (*b*) lines of constant toroidal function w on the outer surface of the fluid shell are shown for $T = 10^4$, $R = 2950$ and $m_0 = 2$; (*c*) and (*d*) are the same as (*a*) and (*b*) but for $m_0 = 4$. The solid contours of the zonal flow indicate eastward azimuthal motion and the dashed contours denote westward motion.

Since a three-dimensional nonlinear solution is composed of three scalar functions without exact stream functions, it is difficult to clearly illustrate a solution of complicated nonlinear convection with only a small number of figures. However, it appears that the toroidal stram function w and the contours of heat flux $H_r = -\partial\Theta/\partial r$ both plotted on the outer spherical surface of the fluid shell can be used to show general features of the convection pattern, and that streamlines of axisymmetric poloidal flow

$$\Psi = -\sum_{l,n} v_{i0n} \sin\theta \sin n\pi(r-r_i) \frac{\partial Y_l^0}{\partial\theta},$$

and the contours of axisymmetric toroidal flow

$$U_\phi = -\sum_{l,n} w_{l0n}\, r \cos{(n-1)}\, \pi(r-r_i)\, \frac{\partial Y_l^0}{\partial \theta},$$

in a meridional cross-section can be used to demonstrate the average features of the flow. The radial component of velocity $u_r = \mathrm{L}^2 v/r$ on a spherical surface in the fluid shell within the range of parameters studied is well correlated with the field of heat flux $-\partial\Theta/\partial r$ on the outer surface of the shell, that is, hot fluid rises while cold fluid sinks. Consequently, the plot for poloidal radial flow on a spherical surface in the fluid shell can be omitted without losing any information on poloidal flows. Thus, in this paper four different figures, two on the outer surface and two on the meridional cross section, in the drifting frame of reference in which the solution is either stationary or vacillatory, are chosen to represent the principle spatial features of a nonlinear solution.

Multiplicity of steady solutions is a typical feature of the nonlinear convection which can sometimes provide valuable insight into the more complicated states, as we will discuss in §6, where convection vacillates between two competing states characterized by different dominant wavenumbers. For the same parameters, $R > 1994$ and $T = 10^4$, the $m_0 = 4$ nonlinear solutions can bifurcate from the most unstable mode with $m_c = 4$ at $R_c = 1697$, while the $m_0 = 2$ solutions can bifurcate from the higher mode with $m_c = 2$ at $R_c = 1994$. In figure 2, the two primary solutions at $T = 10^4$ and $R = 2950$ with the different dominant wavenumbers $m_0 = 2$ and 4 are chosen as a typical example to illustrate their different structures. The difference in the characteristics of non-axisymmetric components shown in figure 2(*b*, *d*) is as expected from the linear theory. Especially noticeable in the figures, however, is the axisymmetric structure, where a predominant single-cell thermal wind develops in the lower latitude for the $m_0 = 2$ solution while the meridional circulation with a double-cell structure in mid-latitude characterizes the $m_0 = 4$ solution. The axisymmetric azimuthal flows generated by the interaction of the meridional flow and the Coriolis force display accordingly the different structure in higher latitude.

4. Instabilities of steadily drifting convection

Nonlinear primary solutions bifurcating from the trivial solutions of instabilities are usually dominated by the modes that are most unstable at the onset of convection. One of the interesting questions in nonlinear convection is how the nonlinear processes overcome various constraints associated with the effects of rotation. The instability analysis of the nonlinear solutions will shed some light on the answer because the form of new bifurcation solutions can usually be inferred from the structure and the symmetry of the most rapidly growing perturbation.

The loss of or change in symmetry of a solution arising from instabilities and the nature of the new bifurcating solutions are often closely related. It has been shown that a proper understanding of the nature of symmetry breaking in a simple plane layer geometry can be very complex, and requires a group-theoretical approach (McKenzie 1987). In comparison, rotating spherical convection has much simpler symmetry properties which are of great advantage for numerical treatments of the problem. A primary solution bifurcating from the spherically symmetric static state possesses three basic symmetries: the symmetry with respect to the equatorial plane, the symmetry with respect to azimuthal periodicity in connection with an azimuthal

wavenumber m, and the time symmetry in the sense that solutions are steady in the reference of a drifting frame. Accordingly, solutions of the stability analysis for the system of equations (4)–(6) can be separated into three classes. The first class of perturbation, which is antisymmetric with respect to the equatorial plane, is unlikely to be significant in the region of parameter space treated in this paper as clearly shown in figure 1. Disturbances of the second type possesses the same symmetry and same spatial structures as the corresponding nonlinear solution, and are characterized by the parameter $M = 0$. The instability in connection with the latter type of disturbances usually leads to a vacillating convection through Hopf-type bifurcation from steadily drifting convection. However, the Eckhaus-type instability also could occur for this class of disturbances because the wavenumbers $m = jm_0$, where j is an integer, are included in the nonlinear calculation. The third class of solutions for (4)–(6) differs from the second in that the growing perturbation, with a finite value of the parameter M, tends to change the spatial scale and structure of the steadily drifting convection.

To investigate the stability of $m_0 = 4$ nonlinear travelling wave solutions at $T = 10^4$, which bifurcate from the most unstable linear mode, three different types of the equatorially symmetric disturbances as well as the equatorially antisymmetric disturbances have been used to perturb the nonlinear solutions. With $M = 0$, the azimuthal wavenumbers of the related disturbance $\tilde{\boldsymbol{u}}$ include

$$m = 0, 4, 8, 12 \ldots,$$

and the disturbance $\tilde{\boldsymbol{u}}$ with $M = 2$ includes

$$m = 2, 6, 10, 14 \ldots$$

in the expansions. The disturbances described by $M = 1$ and $M = 3$ are identical and contain the following wavenumbers

$$m = 1, 3, 5, 7 \ldots$$

The largest growth rate, σ_r, of the infinitesimal perturbations corresponding to $M = 2$ and 3 for the $m_0 = 4$ nonlinear solutions at $T = 10^4$ is displayed as a function of R in figure 3. The instability boundaries corresponding to $M = 0$ and the antisymmetric perturbation are at much higher values of R, and are therefore not shown in the figure. The results of the stability analysis meet the expectation that the interaction between the two spatially resonant wavenumbers $m = 2$ and 4 is much stronger than the interaction between the non-resonant wavenumbers $m = 3$ and 4. For a Rayleigh number R slightly above the critical value R_c, the system (4)–(6) with different M describes approximately the linear onset of convection. The linear behaviour that $R_c(m = 3)$ is much closer to $R_c(m = 4)$ than $R_c(m = 2)$ as shown in figure 1 is clearly manifested in figure 3. As the amplitude of the nonlinear solutions increases, the perturbation dominated by $m = 2$ modes grows much faster than the one dominated by $m = 3$. All initial infinitesimal disturbances characterized by $M = 3$ to the $m_0 = 4$ nonlinear solutions are damped and decay to zero with increasing time in the parameter range considered in this paper. The odd-wavenumber modes have therefore been disregarded for the non-linear solutions of higher bifurcations. The fastest growing $M = 2$ disturbance and its associated structure indicate that the additional scales characterized by the prevailing azimuthal wavenumber $m = 2$ will be introduced to the primary solutions by the instability. Of particular interest, however, is that the largest growth rate of the infinitesimal perturbation is real, that is, $\sigma_i = 0$. Therefore, the spatial symmetry is

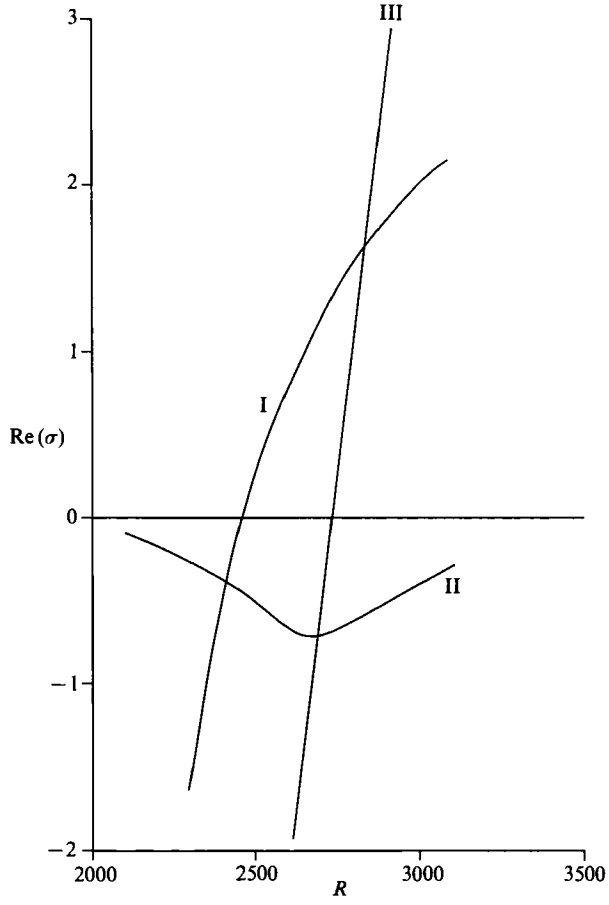

FIGURE 3. Curve I gives the largest real part of the growth rate with the $M = 2$ disturbance for the $m_0 = 4$ solution, and curve II corresponds to the $M = 3$ disturbance. Curve III represents the largest growth rate from the instability analysis of the mixed-mode solution.

broken by the instability, but the time symmetry is preserved. A secondary new solution in the form of steadily drifting cells, with the mixed predominant wavenumbers $m_0 = 2$ and 4, as suggested by the instability, may bifurcate from the steadily drifting solution of $m_0 = 4$. This new type of solution will be termed *mixed-mode convection*.

We now turn to the stability properties of the $m_0 = 2$ nonlinear solutions, which are not related to the most unstable linear mode. Figure 4 shows the real part of the growth rate of the fastest growing disturbance as a function of Rayleigh number R for finite-amplitude solutions that bifurcate from the trivial solution with $m_0 = 2$ at $T = 10^4$. Infinitesimal perturbations to the steadily drifting state will grow in time for $R < 2900$. The structure of the critical disturbance shows that the fastest growing modes are characterized by the azimuthal wavenumber $m = 4$ as we expect from the linear theory. The underlying instability mechanism is of the Eckhaus-type that restricts the stable wavenumber in the neighbourhood of the critical wavenumber. The steadily drifting solutions with four cells give way to the solutions with eight cells when the amplitude of the former solution is small. The interpretation of the Eckhaus-type instability is supported by the fact that the imaginary part of fastest

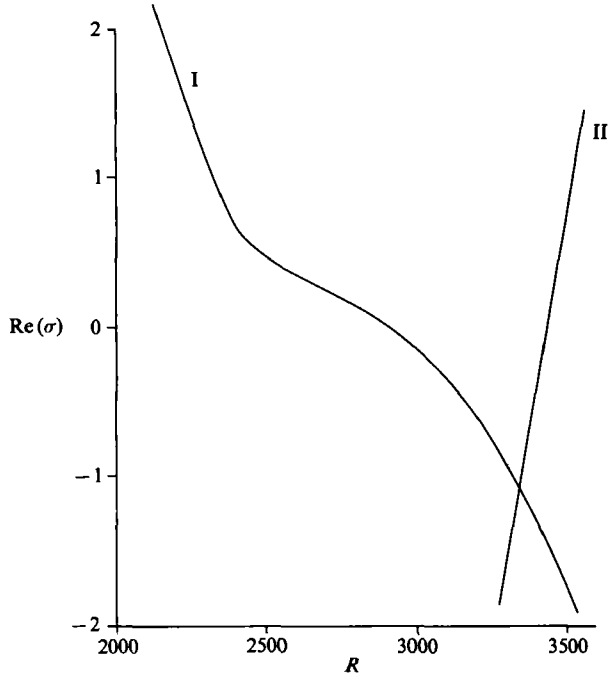

FIGURE 4. Real part of the growth rate σ as a function of Rayleigh number R from the linear stability analysis for $T = 10^4$ and $m_0 = 2$. Curve I represents the instability due to the most rapidly growing $m_0 = 4$ disturbance and curve II the amplitude-vacillation instability.

growth rate, σ, of the disturbance related to the Eckhaus-type instability can be approximately given by

$$\sigma_i = m(c_2 - c_4),$$

where c_2 and c_4 represent the drifting rate of $m_0 = 2$ and $m_0 = 4$ nonlinear convection. For instance, $c_2 = 4.66$ and $c_4 = -0.19$ for $T = 10^4$, $R = 2200$, gives the predicted imaginary growth rate $\sigma_i = 19.5$ while the actual value from the instability analysis is $\sigma_i = 20.49$. The most interesting feature of this stability analysis is the decreasing growth rate σ_r (line I in figure 4) with increasing Rayleigh number R. When $R > 2900$, the perturbations characterized by a fastest growing mode with $m = 4$ decay in time, that is, the $m_0 = 2$ nonlinear solutions which are unstable at small amplitudes become stable at larger amplitudes. The essential aspect of this behaviour is the competitive constraints imposed by rotation and the nonlinearity of the flows. The most unstable linear wavenumber of the system is chosen as the optimum balances among the Coriolis force, the pressure gradient and the viscous dissipation with the spherically symmetric buoyancy force. It seems most likely that the nonlinear modification to the spherically symmetric temperature distribution, which promotes the axially symmetric distribution, provides the key influence of finite-amplitude effects. As the new distribution of buoyancy forces drives convection more effectively, the large scale convection with $m_0 = 2$ eventually gains stability through nonlinearity even when the $m_0 = 4$ solution is much preferred at the onset (see figure 1). As the Rayleigh number, R, further increases, the stable $m_0 = 2$ drifting solution loses its stability at about $R = 3400$, represented in curve II of figure 4, to the amplitude-vacillating instability that leads to a periodic fluctuation in the amplitude of flows but with little change in the shape of convection pattern. The behaviour of this instability is the same as for the instability of the $m_0 = 2$ solution

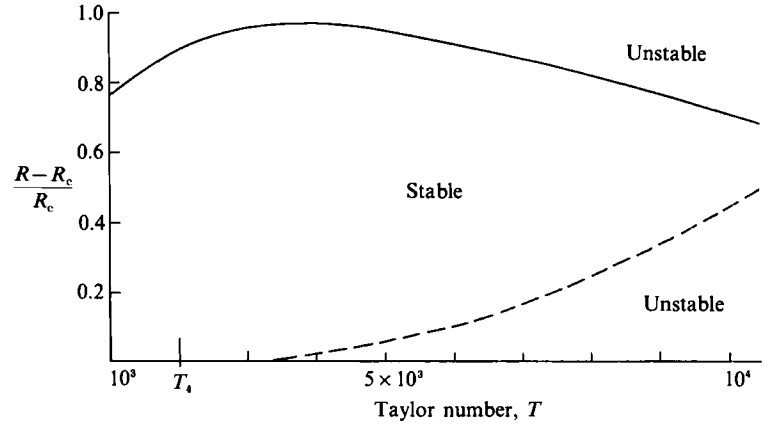

FIGURE 5. Stability diagram for $m_0 = 2$ solutions. The dashed curve corresponds to the stability gained owing to nonlinearity, and the solid curve indicates the amplitude-vacillating instability.

at a lower Taylor number. The eigenfunction associated with the most rapidly growing mode displays the same structure as the $m_0 = 2$ primary solution, which suggests an amplitude-vacillating solution for the higher bifurcation.

After showing the instabilities at a representative Taylor number, it would be profitable to see the dependence of instabilities on the Taylor number. The stability diagram for the $m_0 = 2$ steadily drifting solutions is shown in figure 5 in which the supercritical Rayleigh number $(R-R_c)/R_c$ is plotted against Taylor number T. The instability curves are based on extensive computations for nonlinear drifting solutions at the Taylor numbers $T = 10^3$, 1.2×10^3, 2.0×10^3, 4.0×10^3, 6.0×10^3, 10^4, 2.0×10^4 and 5.0×10^4. About 20 nonlinear solutions for each Taylor number have been obtained for the Rayleigh numbers $R_c < R < 3R_c$. The stability analysis is performed on every solution, and the results are used to extrapolate the actual instability boundaries. In figure 5, T_4 indicates the critical Taylor number beyond which the $m_0 = 4$ solutions become preferred according to the linear theory. The dashed curve corresponds to the boundary of stability resulting from the finite-amplitude effects of convection. This new stability is referred to as *the stability of finite amplitude*. The amplitude-vacillation instability is given by the solid line. The steadily drifting convection with the predominant wavenumber $m_0 = 2$ is stable with respect to the even-wavenumber disturbances within the parameter space bounded by the dashed and solid curves. However, the domain of stable $m_0 = 2$ solutions is likely to be more restricted if the disturbances with $M = 3$ are admitted. Within the region of the dashed curve and the line of $(R-R_c)/R_c = 0$, the steadily drifting convection with $m_0 = 4$ can be stable. Because of the stability of finite amplitude, the wavenumber of the most unstable mode at the onset of convection does not necessarily correspond to the dominant wavenumber of finite-amplitude convection, even at weak nonlinearity. For instance, at the Taylor number $T = 3T_4$, the $m_0 = 2$ solution gains stability at $R = R_c + 0.1R_c$. It has been reported in many laboratory experiments on rotating fluids (e.g. Hide & Mason 1975; Chamberlain & Carrigan 1986) that the observed dominant wavenumber m_0 observed at finite supercriticality is smaller than the theoretically predicted values even though the critical parameter, such as the critical Rayleigh number R_c is in a good agreement with the linear theory. Discrepancies between the experiments and theory are likely to be attributable to the stability of long-wavelength solutions gained by nonlinear effects on rotating fluid systems. The parameter range of stable nonlinear convection with the dominant

wavenumber $m_0 = 2$ appears to be much wider than that predicted from the linear analysis owing to the stability of finite amplitude of convection.

5. Steadily drifting mixed-mode convection and its stability

The linear stability analysis of the previous section suggests that mixed-mode solutions with two competing scales of convective cells emerge from the $m_0 = 4$ drifting solution. Secondary bifurcation solutions in the neighbourhood of the bifurcation point may be assumed to have the form

$$\boldsymbol{u} = \boldsymbol{u}_0 + \epsilon \tilde{\boldsymbol{u}}, \tag{7}$$

where the $\tilde{\boldsymbol{u}}$ is the eigenvector associated with the strongest growth rate of the perturbation and ϵ is a small parameter that depends on the supercritical Rayleigh number $R - R_{1c}$. R_{1c} denotes the critical Rayleigh number for the instability of steadily drifting convection determined by the linear stability analysis. We have taken $\epsilon = C(R-R_{1c})^{\frac{1}{2}}$, where C varies between 0.001 to 0.1, depending on the parameters T and R. Iterating (1)–(3) with the Newton–Raphson method by changing the parameter ϵ, a new form of steadily drifting solution can be obtained if (7) gives rise to an approximate solution of the new branch. The value of the parameter ϵ usually indicates whether the bifurcation is supercritical or subcritical. If the bifurcation is supercritical, the stability of solutions determined by the linear stability analysis in the previous sections is both necessary and sufficient. We found that the iterating parameter ϵ can be set to be numerically approaching zero for a correspondingly small positive value of the supercritical Rayleigh number $R - R_{1c} = \epsilon^2/C^2$. The bifurcation is apparently supercritical. Otherwise a negative value of ϵ^2/C^2 must be used for iterations for a subcritical bifurcation as shown in the case of lower Prandtl numbers (Zhang & Busse 1988). Once we have a first secondary solution, other solutions in the parameter space can be easily and cheaply generated by iteration toward the neighbouring parameters of the system.

An impression of the pattern of the new solutions can be gained from figure 6 at $T = 10^4$ and $R = 2950$. Since the parameters of the solutions used in figure 6 are precisely the same as in figure 2, the differences among these three nonlinear solutions which are dominated by either $m_0 = 2$ or 4, or by the combination of $m_0 = 2$ and 4, are clearly illustrated by comparing these figures. From the figures it can be seen that the profile of the mixed-mode convection, as we should expect, is eventually a combination of the patterns of $m_0 = 2$ and 4 nonlinear solutions. The pattern of heat flux in figure 6 (*a*) displays the typical features of the $m_0 = 4$ solution which is dominated by the modes of the azimuthal wavenumber $m = 4$, while the non-axisymmetric structure of the toroidal flows is clearly dominated by the modes of the $m_0 = 2$ solution. The meridional circulation shown in figure 6 (*c*) resembles the profile of the $m_0 = 2$ convection. Accordingly, there is very little difference between the mean zonal flows of the mixed-mode solution and that of the $m_0 = 2$ solution. Further comparison of the three types of solutions can be made by considering global properties which measure the vigour of nonlinear motion. Introducing the average kinetic energy density of different components of velocity $\boldsymbol{u}$,

$$\bar{E}_w = \Gamma \int (\mathrm{d}v)\, \nabla \times r\bar{w} \cdot \nabla \times r\bar{w}, \tag{8}$$

$$\tilde{E}_w = \Gamma \int (\mathrm{d}v)\, \nabla \times r\tilde{w} \cdot \nabla \times r\tilde{w}, \tag{9}$$

$$\bar{E}_v = \Gamma \int (\mathrm{d}v)\, \nabla \times r\bar{v} \cdot \nabla \times r\bar{v}, \tag{10}$$

$$\tilde{E}_v = \Gamma \int (\mathrm{d}v)\, \nabla \times r\tilde{v} \cdot \nabla \times r\tilde{v}, \tag{11}$$

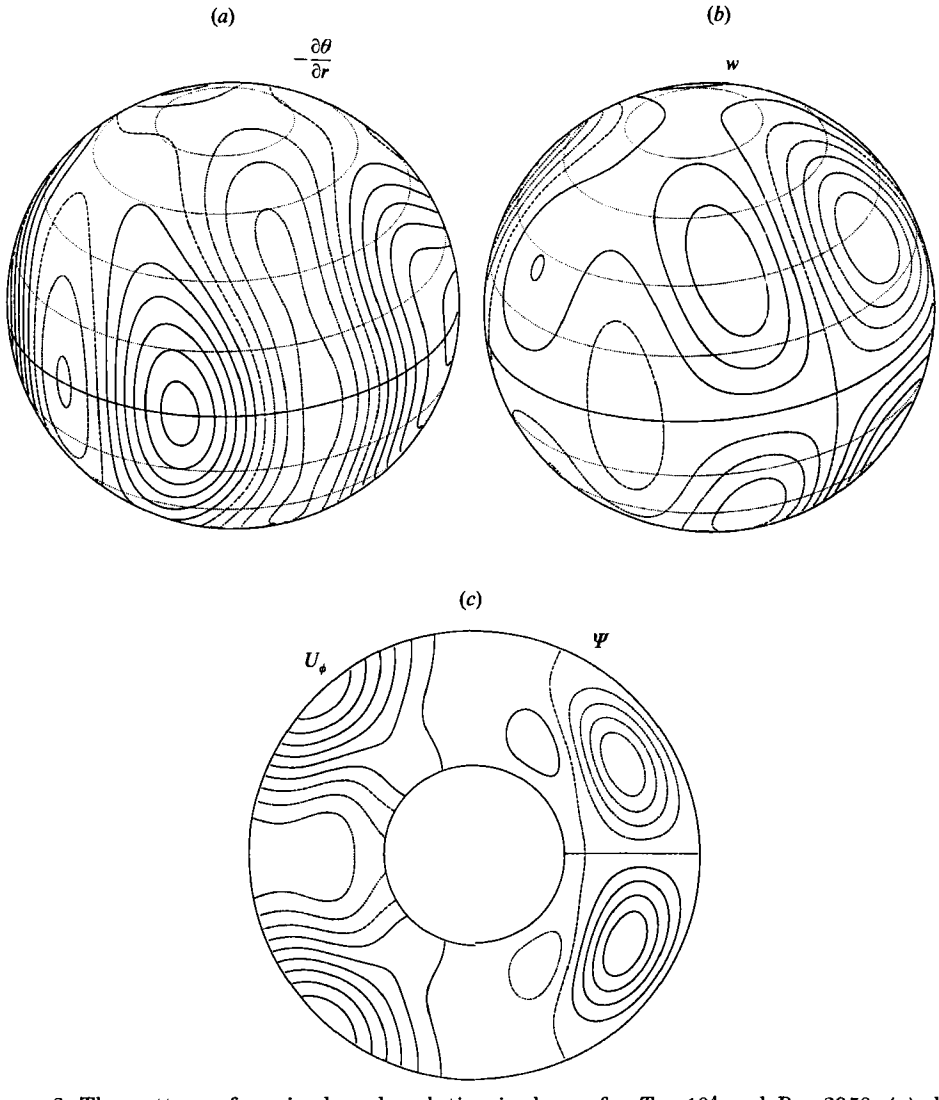

FIGURE 6. The pattern of a mixed-mode solution is shown for $T = 10^4$ and $R = 2950$. (*a*) shows contours of the heat flux on the outer surface; (*b*) and (*c*) are the same as figure 2 (*a*, *b*) but for the mixed-mode solution.

where $\Gamma = 3(1-\eta)^3/2\pi(1-\eta^3)$, and the overbar indicates the axisymmetric components of flow and the tilde the non-axisymmetric components. The $\int(\mathrm{d}v)$ represents the integral over the spherical fluid shell. The measure of heat transfer by convection can be provided by the total outer heat flux

$$H_o = -\partial\langle\bar{\Theta}\rangle/\partial r$$

at $r = r_o$, the symbol $\langle\ \rangle$ denoting the integral over the surface of the fluid shell. Its relationship with the outer Nusselt number Nu_o is

$$Nu_o = 1 + (1-\eta)H_o.$$

The spectrum of kinetic energy densities of various components as well as the heat flux H_o for the three steadily drifting nonlinear solutions for the same parameters at

Energy	$m_0 = 2$	$m_0 = 4$	Mixed-mode
$\bar{E}_v, m = 0$	0.04	0.14	0.03
$\tilde{E}_v, m = 2$	9.87	0	3.15
$\tilde{E}_v, m = 4$	0.56	14.79	7.03
$\tilde{E}_v, m > 4$	0.13	0.25	1.33
$\bar{E}_w, m = 0$	0.88	0.22	0.46
$\tilde{E}_w, m = 2$	34.24	0	10.27
$\tilde{E}_w, m = 4$	0.93	25.70	12.46
$\tilde{E}_w, m > 4$	0.07	0.07	0.89
H_0	0.12	0.22	0.16

TABLE 1. Energy spectra and heat flux for the three different nonlinear solutions at $T = 10^4$ and $R = 2800$. Quantities are defined in equations (8)–(11).

N_t	R_c, ω_c	R_{c2}	σ_{i2}	$H_0(R = 2800)$	$\sigma_n(R = 2800)$
3	1698.1, −1.936	2648	9.4	0.157	8.02
4	1696.8, −1.895	2716	9.1	0.160	7.85
5	1697.1, −1.886	2704	8.7	0.167	7.90
6	1697.0, −1.888	2709	8.6	0.162	8.05

TABLE 2. The convergence behaviour with increasing truncation parameter N_t. σ_{i2} represents the imaginary part of growth rate for the most rapidly growing disturbances at R_{c2}. H_0 is the outer heat flux of the mixed-mode solution, and σ_n is the frequency of wavenumber-vacillating convection obtained from numerical integration.

$R = 2800$ and $T = 10^4$ are shown in table 1. The Rayleigh number is chosen to be near its instability boundary for both the $m_0 = 2$ and mixed-mode drifting solutions. The energy spectra display a distinct change of character between the secondary mixed-mode convection and the m_0 primary solution, though both are steadily drifting with constant amplitude. The main features of the spectra are consistent with those reflected in the pattern of the nonliner flows displayed in figures 2 and 6. The kinetic energies of the $m_0 = 2$ and 4 solutions are dominated by the contributions from their fundamental modes, and the higher modes $m > m_0$ have less than 5% of the total energies. For the mixed-mode solution a considerable amount of kinetic energy is transferred from the $m = 4$ to the competing scale (wavenumber $m = 2$) of the flow. The kinetic energies contained in competing wavenumbers $m = 2$ and $m = 4$ are comparable. It is also of interest to note that both the toroidal and poloidal axisymmetric components of the mixed convection are dominated by the mode of the $m_0 = 2$ solution, although the kinetic energy contained in the modes of $m = 4$ is larger than that of $m = 2$.

Close competition between the two fundamental modes suggests that the mixed-mode solution will lose stability as R increases further. In attempting to find the stability properties of mixed-mode convection, the computations to obtain many mixed-mode solutions for different Rayleigh number R are first carried out. This is followed by linear stability analysis for every solution. The actual stability boundary, denoted by R_{2c}, can then be interpolated. The convergence behaviour of the solutions is displayed in table 2. The refinement of accuracy at the $N_t = 6$ truncation level, which includes about five times the number of modes as the $N_t = 3$ truncation level, shifts the instability boundary slightly without affecting the whole structure. The convergence of the nonlinear solution as well as its stability boundary

are quite convincing. The largest real part of the eigenvalues from the stability analysis of mixed-mode solutions as a function of R is shown in curve III of figure 3. This instability is very robust, and is a result of the strongly growing competing mode associated with the wavenumber $m = 2$ which indicates the transition from a steady mixed-mode drift state to a wavenumber-vacillating state.

6. Convection with vacillating wavenumber and amplitude

The iteration method cannot be used to calculate a vacillating solution, because of the second frequency of the system introduced by the wavenumber- or amplitude-vacillating instability. In the limit of infinite Prandtl number, the implicit time-step scheme must be used as the velocity $\boldsymbol{u}$ responds instantaneously to variations in the temperature field, Θ. The time-step, Δt, is kept small enough to ensure accuracy, while adequate resolution of the vacillating solutions is checked by increasing the number of harmonics included (table 2), as well as different values of the time-step Δt. Taking

$$\boldsymbol{u}(t=0) = \boldsymbol{u}_0 + \epsilon \boldsymbol{u}_s$$

as an initial condition for the time integration of (1)–(3), where $\boldsymbol{u}_0$ is either an unstable mixed-mode or an unstable m_0 drifting solution slightly above the instability boundary. Here $\boldsymbol{u}_s$ represents the fastest growing disturbance from the results of stability analysis. Once the initial transient period is over, time-dependent convection settles down to a periodic vacillation, the period of which is approximately given by $p_0 = 2\pi/\sigma_i$, where σ_i is the frequency of the most rapidly growing disturbance as predicted from the stability analysis. After the first time-dependent solution is obtained for a small value of the supercritical Rayleigh number $R - R_{2c}$, it is used as the initial condition for a vacillating solution with different neighbouring parameter values.

The instability of mixed-mode solutions leads to the tertiary bifurcation in which the predominant wavenumber m_0 varies periodically between two competing neighbouring wavenumbers, $m_0 = 2$ or 4, while the whole pattern of the solution drifts in the azimuthal direction. Our integration indicates that the Hopf-type bifurcation is apparently supercritical. In the immediate neighbourhood of supercritical bifurcation, at $R = R_{2c} + \epsilon^2/C^2$, the kinetic energy and the heat flux H_0 oscillate slightly about the value of the mixed-mode drifting solution. The vacillation grows in amplitude as R increases. By $R = 2800$ at $T = 10^4$ the value of the heat flux H_0 varies by 50 % during a period of oscillation. The phenomenon of the convection with vacillating wavenumber is perhaps most clearly illustrated by separating the $m_0 = 2$ and $m_0 = 4$ contributions, as shown in figure 7 (*a*) for $R = 2950$ and $T = 10^4$. The kinetic energies of the $m_0 = 4$ mode (solid curves) reach their maxima while those for the $m_0 = 2$ mode attain their minima (dashed curves), and vice versa.

Having briefly described the phenomenon of wavenumber vacillation, let us examine the detailed patterns of the wavenumber-vacillating solutions. Figures 8 and 9 illustrate the typical convection patterns at almost equally spaced instants in time during a complete oscillation at $R = 2950$. It should be noted that the whole pattern in these figures drifts azimuthally at a phase speed $c = 4.0$ while the pattern of flows presents a periodic time dependence in which the convection vacillates between the two states with typical wavelengths $2r_0\pi/2$ and $2r_0\pi/4$. Because the fundamental harmonic modes $Y^2_{2,3}$ and $Y^4_{4,5}$ are coupled nonlinearly, the evolution of convection enhances one mode at the expense of the other mode. Comparing the

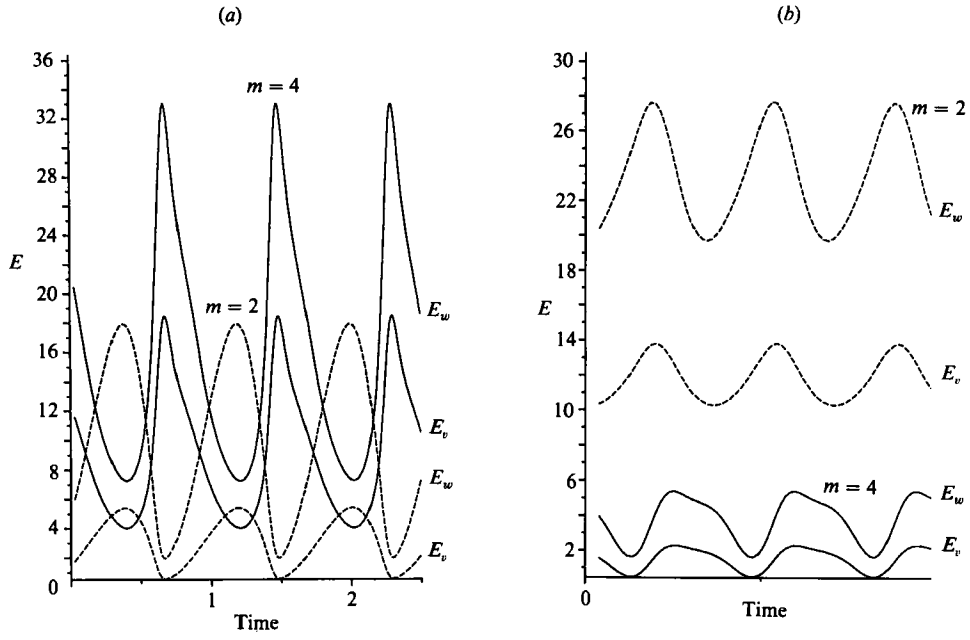

FIGURE 7. The kinetic energies as a function of time for (*a*) the wavenumber-vacillating solution at $T = 10^4$, $R = 2950$, and (*b*) the amplitude-vacillation solution at $T = 1.2 \times 10^3$ and $R = 1840$. The dashed lines represent the $m = 2$ contribution while the solid lines show the $m = 4$ contribution.

axisymmetric zonal flows and the meridional circulation in figure 9 with the $m_0 = 2$ and 4 solutions illustrated in figure 2, the vacillation of convective pattern between the two states of the $m_0 = 2$-type and the $m_0 = 4$-type is quite clearly depicted. The meridional circulation of the vacillation at $t = 3p_0/4$ is almost, although not exactly, the same as the circulation pattern of the $m_0 = 2$ steadily drifting convection. At $t = p_0/4$, the profile of convection is similar to that of the $m_0 = 4$ solution. The flow at this instant is apparently dominated by the $m = 4$ mode, and the corresponding kinetic energies attain their peaks. When the kinetic energies of the $m = 4$ mode reach their minima the pattern of convection displays the $m_0 = 2$-type solution. The spectra of kinetic energy at the instants of peaks and minima are given in table 3.

In order to contrast wavenumber-vacillating convection with amplitude-vacillating convection which is associated with the instability corresponding to the solid curve in the stability diagram in figure 5, we display one time series of amplitude-vacillating solution, again with the $m_0 = 2$ and 4 contributions separated, at $T = 1.2 \times 10^3$, $R = 1840$ and $m_0 = 2$ in figure 7(*b*). Many amplitude-vacillating solutions have been obtained, and they show a very similar behaviour to the case illustrated. A periodic variation in the amplitude of drifting convection constitutes an amplitude vacillation. The corresponding pattern of flow changes very little during the vacillation except for a relatively large fluctuation in the non-axisymmetric poloidal component which is associated with the heat transport.

The phenomena of amplitude and wavenumber vacillation in baroclinically driven flows have been observed in carefully controlled rotating-fluid-annulus experiments. We refer to the review paper by Hide & Mason (1975) for a detailed discussion. A direct comparison between experiments and our analysis is not feasible. However, the basic dynamics in our system and experiments are both constrained by the

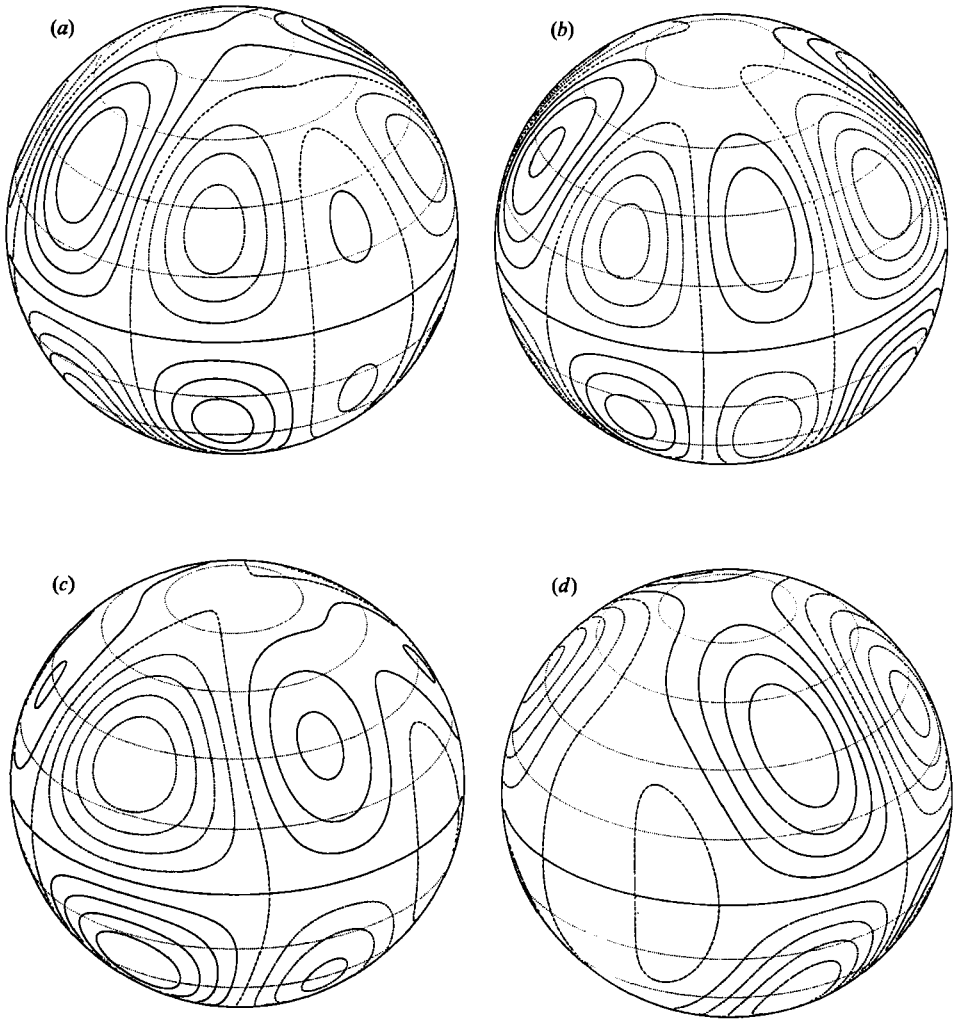

FIGURE 8. Contours of toroidal function w on the outer surface of the fluid shell at almost equally spaced instants in time during a complete vacillation for $T = 10^4$ and $R = 2950$ seen from the drifting frame with a rate $c = 4.0$. (*a*), (*b*), (*c*), (*d*) correspond to the instants at $t = ip_{0/4}$, $i = 0, 1, 2, 3$, respectively.

Coriolis force, and it seems plausible that the physical mechanisms underlying the amplitude and wavenumber vacillations observed in rotating annulus experiments are similar to those described in this paper.

Coupled nonlinear amplitude equations have been widely used to describe the nonlinear interaction of convective modes of different wavenumbers (e.g. Proctor & Jones 1988). Our results, particularly figure 7, suggest that a similar semi-analytical approach, in which linear solutions and coefficients of the cubic terms of the amplitude equations are obtained numerically, may be useful but this has not been attempted. Furthermore, the convection with vacillating wavenumber and amplitude described in this paper can be understood within the framework of the coupled amplitude equations for a much simpler system (e.g. Dangelmayer & Knobloch 1987). Our steadily drifting nonlinear convection corresponds to the travelling wave solution introduced by the first Hopf bifurcation (the onset of

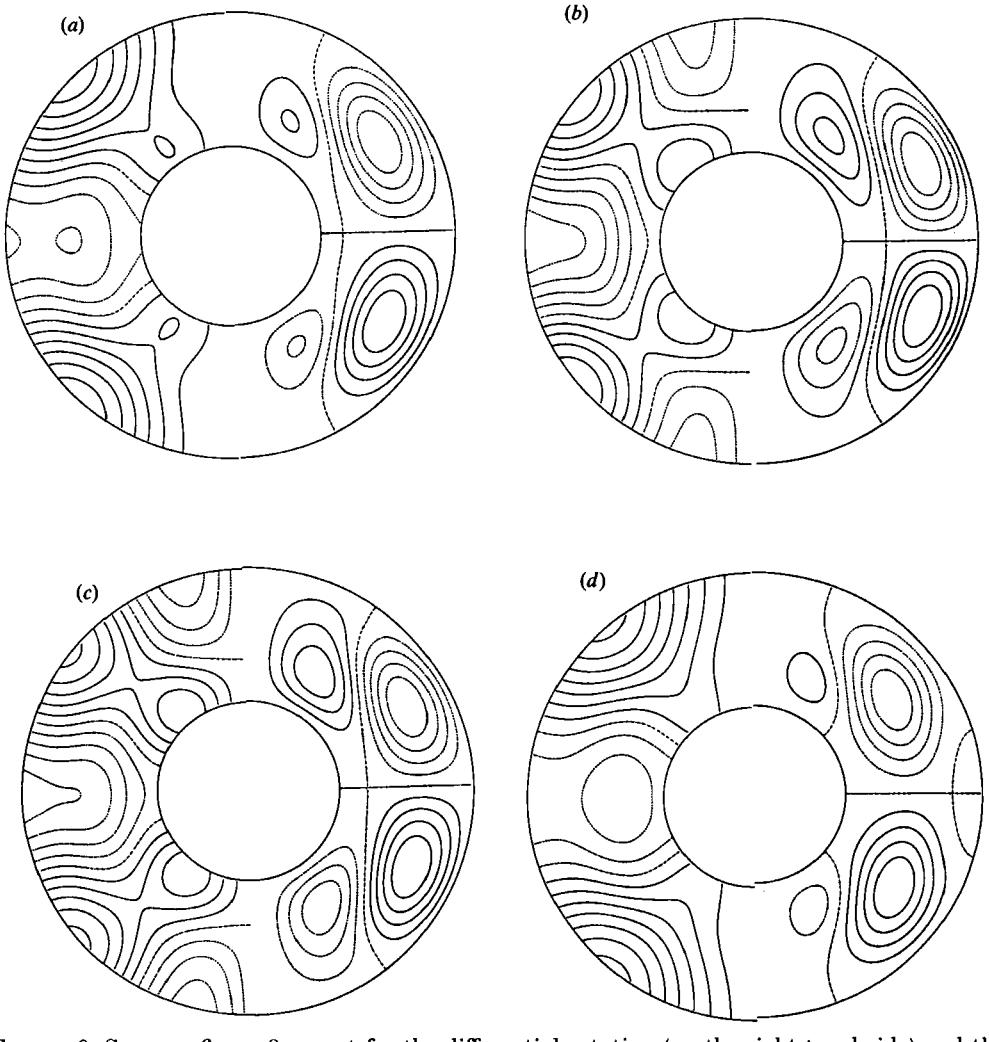

FIGURE 9. Same as figure 8 except for the differential rotation (on the right-hand side) and the meridional circulation (on the left-hand side) at a meridional cross-section.

Energy	At minimum	At maximum
$\bar{E}_v, m = 0$	0.02	0.118
$\bar{E}_v, m = 2$	5.39	0.581
$\bar{E}_v, m = 4$	4.02	18.46
$\bar{E}_v, m > 4$	1.28	0.499
$\bar{E}_w, m = 0$	0.54	1.006
$\bar{E}_w, m = 2$	17.80	1.97
$\bar{E}_w, m = 4$	7.27	33.00
$\bar{E}_w, m > 4$	0.72	0.23

TABLE 3. Energy spectra for wavenumber-vacillating convection at $T = 10^4$ and $R = 2950$ at two instants in time corresponding to the figures 8(*b*), 9(*b*) and 8(*d*), 9(*d*)

convection). The convection with vacillating wavenumber and amplitude (the modulated waves) is introduced by the secondary Hopf bifurcation (wavenumber- and amplitude-vacillating instabilities) with an explicit time dependence. The amplitude-vacillating convection represents a travelling wave weakly modulated by the second travelling wave with a different wavenumber; the wavenumber-vacillating convection is a result of the strong nonlinear interaction of the two travelling waves with different wavenumbers (figure 7).

7. Summary and concluding remarks

We have investigated the temporal and spatial behaviour of three-dimensional convection for a rotating spherical fluid shell in the limit of infinite Prandtl number. The main features of the instabilities and the bifurcation solutions at two representative Taylor numbers were determined for moderate Rayleigh numbers $R < 2R_c$. The associated bifurcation structure has been followed in some detail for the case of $T = 10^4$. The main results at $T = 10^4$ are summarized in the bifurcation diagram in figure 10. The steadily drifting primary solution with $m_0 = 4$, denoted by the M_4 branch, with a relative simple spatial pattern, loses its stability which leads to the steadily drifting branch M_{24} with a much more complicated spatial structure involving the two competing dominant wavenumbers $m_0 = 2$ and 4. The amplitude and heat transfer for both branches are independent of time. The branch V_{24} emerges supercritically from the steadily drifting mixed-mode branch and is characterized by the vacillation between the two competing scales of spatial structures. Since the Nusselt number Nu_0 is a function of time, the value shown in the bifurcation diagram is averaged over the period of vacillation. The amplitude-vacillating solution is represented by the branch V_2.

The fact that stable branch M_2 exists at large amplitudes for a high supercritical Taylor number $T > T_4$ indicates that the competition between the constraints of rotation and nonlinear modifications of the spherically symmetric driving forces can be of fundamental importance in determining the behaviour of nonlinear convection in a rotating system. The comparison of the branches M_4, M_{24} and V_{24} yields the interesting result that the heat transport by convection does not play a critical role in the stability and character of rotating nonlinear convection. The predominant modes for the branches M_{24}, M_2 and V_{24} are not associated with the most unstable modes at the onset of convection as in the case of non-rotating spherical convection (Young 1974). Direct comparisons with the previous numerical studies cannot be made because of the limit of infinite Prandtl number and lower Rayleigh numbers. However, it should be noted that some of the complicated behaviour in rotating spherical convection can be understood in terms of a variety of instabilities that break various symmetries of the convection and occupy available degrees of freedom, in analogy with the various transitions in plane layer convection. Because the number of symmetries in rotating sphere is small and the wavenumbers are integer, following the evolution of nonlinear convection in rotating spherical systems can be numerically much simpler than in a fluid layer.

The system also displays a rich time-dependent behaviour with a transition from the wavenumber vacillation through a period-doubling cascade to chaos when a lower value of the truncation parameter N_t is used. However, as we refine the resolution of solutions, we find the wavenumber vacillation unchanged but the period-doubling bifurcation disappears. Transition to quasi-periodic and chaotic behaviour appears to be sensitive to the higher-order harmonics though they

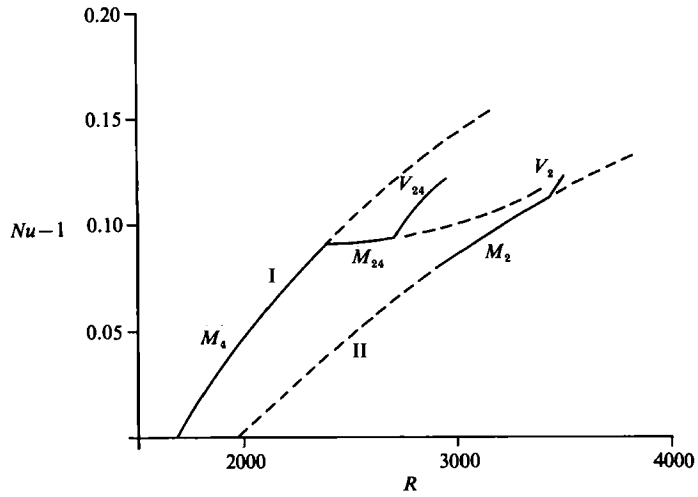

FIGURE 10. Bifurcation diagram for $T = 10^4$. Solid lines correspond to stable solutions, and dashed curves indicate unstable branches. Sequence I: stable steadily drifting convection with $m_0 = 4$ (M_4) ⇒ stable mixed-mode convection (M_{24}) ⇒ wavenumber-vacillating convection (V_{24}). Sequence II: unstable steadily drifting convection with $m_0 = 2$ ⇒ stable steadily drifting convection (M_2) with $m_0 = 2$ ⇒ amplitude-vacillating convection (V_2). All bifurcations are found to be supercritical.

contribute only a small fraction of the total kinetic energy of convection. We have not yet sought time-dependent solutions beyond $R = 3000$ at a higher level of the truncation owing to the very large amount of computer time and storage required.

The only nonlinearity of the problem in the limit of infinite Pr is from the advection of temperature Θ by the flow $\boldsymbol{u}$. An important question to be answered is whether or not the vacillation phenomena studied in this paper have some bearing on the general behaviour of the convection of rotating spherical fluid. Plans for future research will consist of an extension of the studies to moderate or smaller Prandtl numbers in which the momentum advection term plays a important role; another important extension for future research will be to solve the problem of convection at much higher, geophysically relevant, Taylor numbers.

I would like to thank the Leverhulme Trust for a Research Fellowship. I am indebted to Dr M. R. E. Proctor for helpful discussions and to Professor D. Gubbins who has provided many useful comments on the earlier version of the paper. A portion of the computational code was written and tested at the University of Bayreuth, Germany, supported by the Deutsche Forschungsgemeinschaft under Grant BU-589. I would also like to thank Professor F. Busse for numerous discussions. The early part of the work was carried out at the Department of Earth Sciences, University of Cambridge.

REFERENCES

BRAGINSKY, S. I. 1963 Constructure of the F layer and reasons for convection in the Earth's core. *Dokl. Akad. Nauk SSSR* (Engl. transl.) **149**, 1311–1314.

BUSSE, F. H. 1970 Thermal instabilities in rapidly rotating systems. *J. Fluid Mech.* **44**, 441–460.

BUSSE, F. H. 1978 Nonlinear properties of thermal convection. *Rep. Prog. Phys.* **41**, 1929–1967.

CARRIGAN, C. R. & BUSSE, F. H. 1983 An experimental and theoretical investigation of the onset of convection in rotating spherical shells. *J. Fluid Mech.* **126**, 287–305.

CHAMBERLAIN, J. A. & CARRIGAN, C. R. 1986 An experimental investigation of convection in a rotating sphere subject to time varying thermal boundary conditions. *Geophys. Astrophys. Fluid Dyn.* **41**, 17–41.

CHANDRASEKHAR, S. 1961 *Hydrodynamic and Hydromagnetic Stability*. Clarendon.

DANGELMAYR, G. & KNOBLOCH, E. 1987 The Takens–Bogdanov bifurcation with $O(2)$-symmetry. *Phil. Trans. R. Soc. Lond.* A **322**, 243–279.

GILMAN, P. A. 1975 Linear simulations of Boussinesq convection in a deep rotating spherical shell. *J. Atmos. Sci.* **32**, 1331–1352.

GILMAN, P. A. 1977 Nonlinear dynamics of Boussinesq convection in a deep rotating spherical shell. I. *Geophys. Astrophys. Fluid Dyn.* **8**, 93–135.

GUBBINS, D. 1977 Energetics of the earth's core. *J. Geophys.* **43**, 453–464.

HART, J. E., GLATZMAIER, G. A. & TOOMRE, J. 1986 Space-laboratory and numerical simulations of thermal convection in a rotating hemispherical shell with radial gravity. *J. Fluid Mech.* **173**, 519–544.

HIDE, R. 1958 An experimental study of thermal convection in a rotating fluids. *Phil. Trans. R. Soc. Lond.* A **250**, 442–478.

HIDE, R. & MASON, P. J. 1975 Sloping convection in a rotating fluid. *Adv. Phys.* **24**, 47–100.

LOPER, D. E. 1978 The gravitationally powered dynamo. *Geophys. J. R. Astron. Soc.* **54**, 389–404.

MCKENZIE, D. 1987 The symmetry of convective transitions in space and time. *J. Fluid Mech.* **191**, 287–339.

PROCTOR, M. R. E. & JONES, C. A. 1988 The interaction of two spatially resonant patterns in thermal convection. Part 1. Exact 1:2 resonance. *J. Fluid Mech.* **188**, 301–335.

ROBERTS, P. H. 1968 On the thermal instability of a self-gravitating fluid sphere containing heat sources. *Phil. Trans. R. Soc. Lond.* A **263**, 93–117.

YOUNG, R. E. 1974 Finite amplitude thermal convection in a spherical shell. *J. Fluid Mech.* **63**, 695–721.

ZHANG, K. 1991 Spiralling columnar convection in rapidly rotating spherical fluid shells. *J. Fluid Mech.* (submitted).

ZHANG, K. & BUSSE, F. 1988 Finite amplitude convection and magnetic field generation in a rotating spherical shell. *Geophys. Astrophys. Fluid Dyn.* **44**, 33–53.

ZHANG, K. & BUSSE, F. 1989 Convection driven magnetohydrodynamic dynamos in rotating spherical shells. *Geophys. Astrophys. Fluid Dyn.* **49**, 97–116.

ZHANG, K. & BUSSE, F. 1990 Generation of magnetic fields by convection in a rotating spherical fluid shell of infinite Prandtl numbers. *Phys. Earth Planet. Inter.* **59**, 208–222.

ZHANG, K., BUSSE, F. & HIRCSHING, W. 1989 Numerical models in the theory of geomagnetisim. In *Geomagnetism and Paleomagnetism* (ed. F. J. Lowes *et al.*), pp. 347–358. Kluwer.